Optimization and Interfacial Microstructural Mechanisms of Double-Walled ST52/GGG70 Tube Joining via Slight Hydroforming

Reza Mansourian [a], Masoud Mahmoodi [a, *]

a. Faculty of Mechanical Engineering, Semnan University, Semnan, Iran

* Corresponding author: mahmoodi@semnan.ac.ir (M. Mahmoodi).

Keywords

Double walled cylindrical tube;
ST52 steel;
GGG70 cast iron;
Joining;
Response surface methodology

Abstract

In this study, slight hydroforming is introduced as a localized, low-pressure deformation technique for joining double-walled tubes, where controlled radial deformation rather than full tube forming produces a mechanically interlocked ST52/GGG70 interface. A Box–Behnken response surface methodology (RSM) was employed to evaluate the effects of applied forming load (expressed as equivalent internal pressure), forming temperature (25–75 °C), and Nano-Al_2O_3 concentration (0–10 wt%) on the greatest diameter reduction (D1). The analysis revealed that the applied forming load contributed 62.4% of the total effect on D1, followed by temperature (23.1%) and nanofluid content (14.5%). The developed quadratic model exhibited excellent predictive capability (R^2 = 0.9874), and the optimal parameters (≈520 MPa, 73 °C, and 5.6 wt% Nano-Al_2O_3) resulted in a maximum diameter reduction of approximately 14.2%, consistent with the model prediction. Microscopy of specimens produced under optimized conditions revealed a wavy interfacial morphology with an average waviness amplitude of 18–25 µm, accompanied by a thin and discontinuous 3–6 µm intermetallic layer. This interfacial configuration effectively disrupts crack propagation paths and enhances joint integrity. Overall, the results demonstrate that optimized slight hydroforming enables the formation of a crack-resistant, mechanically interlocked interface, confirming its potential as an efficient and controllable joining technique for multi-material tubular structures.

Highlights

- Slight hydroforming is introduced as a low-pressure, deformation-assisted joining technique for double-walled ST52/GGG70 tubes.
- A Box–Behnken RSM design quantified the effects of applied forming load, temperature, and Nano-Al_2O_3 content on the greatest diameter reduction (D1).
- The applied forming load contributed 62.4% of the total effect on D1, and the optimized parameters yielded a maximum diameter reduction of approximately 14.2%.
- Optimized forming conditions produced a wavy interface with 18–25 µm amplitude and a thin, discontinuous 3–6 µm intermetallic layer, enhancing crack resistance.
- The Nano-Al_2O_3 nanofluid improved lubrication and deformation uniformity, contributing to enhanced interfacial integrity under slight hydroforming.

Graphical Abstract

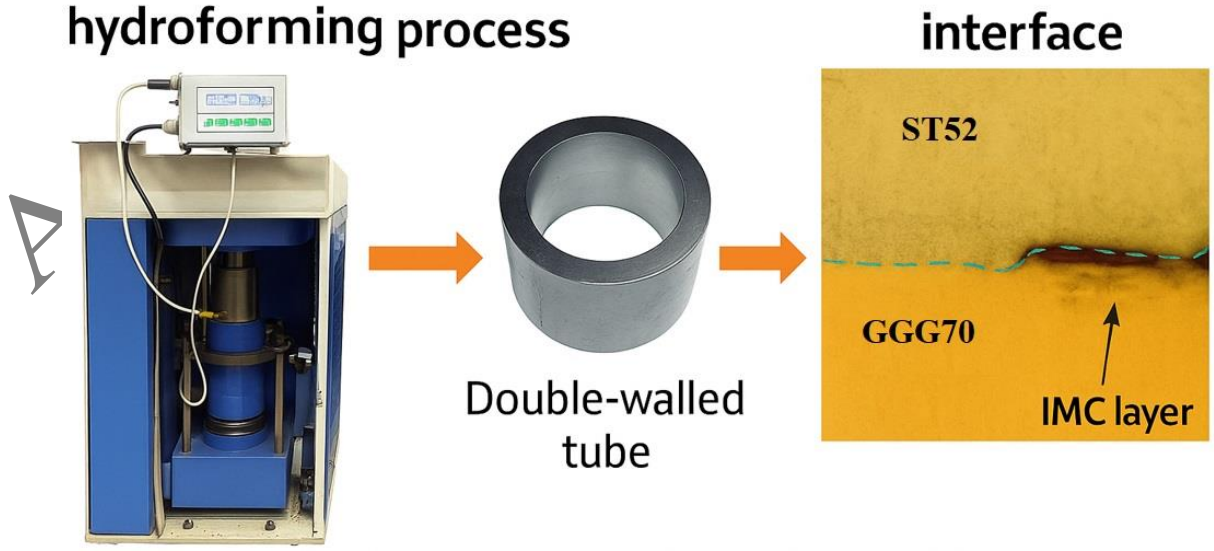

1. Introduction

With the rapid advancement of industries such as fluid transmission, oil and gas systems, chemical processes, and high-temperature heat exchangers, the demand for reliable double-walled cylindrical tubes has significantly increased in recent years [1,2]. Among the various production methods, tube hydroforming is recognized as a widely used technique for manufacturing multilayer pipes due to its capability to form complex geometries with high accuracy [3]. Hydroforming is a pressure-assisted tube-forming process in which internal fluid pressure is applied to shape metallic tubes into desired configurations [4]. The main advantages of this method include the ability to fabricate intricate geometries, reduce the number of components by eliminating welded joints, decrease overall weight, improve surface quality, and enhance mechanical strength [5,6]. Despite these benefits, hydroforming is highly sensitive to process parameters, and improper control may lead to defects such as buckling, wrinkling, excessive thinning, and the development of undesirable residual stresses [7,8]. Therefore, optimizing forming conditions and understanding deformation mechanisms are essential for achieving high-quality products.

Several studies have explored the hydroforming behavior of double-walled tubes. Olabi and Alaswad [9] examined the deformation characteristics of a bi-layer tube with a soft copper inner wall and a harder brass outer layer. Their experiments demonstrated that the combined effect of internal pressure and axial feed significantly improves ductility. In another investigation, Eraslan et al. [10] compared the hydroforming response of single-layer and double-layer tubes under identical test conditions. They used high-purity copper tubes as single-walled specimens, annealed prior to forming, and evaluated the influence of different loading paths through numerical simulations similar to Ref. [9]. Their results emphasized the importance of pressure–feed interaction in controlling deformation. Feng et al. [11] further advanced understanding of multilayer tube hydroforming by optimizing process parameters for forming double-layer Y-shaped tubes using a novel parallel punch system. They analyzed key variables such as internal pressure, axial feed, backward displacement of the punch, and friction coefficient. By examining thinning behavior and contact area evolution, they established optimal loading paths and demonstrated strong agreement between simulation and experimental results, with a maximum deviation of only 5%. This confirms the feasibility and accuracy of systematic optimization approaches in multilayer tube hydroforming.

In the present research, the focus is on evaluating how interface morphology influences the mechanical behavior and interfacial integrity of double-walled tubes composed of ST52 steel (outer tube) and GGG70 cast iron (inner tube). These tubes were initially joined using external pressure, and their interfacial characteristics were subsequently examined after undergoing a slight hydroforming deformation process, designed to produce steel–cast-iron cylindrical tubes. The goal is to assess how deformation-induced microstructural features such as intermetallic layer formation and interface waviness affect interfacial stability and integrity. To clarify the methodology, slight hydroforming in this study refers to a localized, low-pressure variant of tube hydroforming used specifically for joining double-walled tubes rather than shaping their global geometry. In this process, internal pressure is deliberately limited so that only local radial plastic deformation occurs at the ST52/GGG70 interface while the overall tube dimensions remain unchanged. This localized deformation promotes the formation of a wavy, mechanically interlocked interface, contrasting with conventional high-pressure hydroforming aimed at full-tube forming and thickness tailoring. This deformation-assisted joining strategy is consistent with recent developments in plastic-based joining methods for thin-walled metallic tubes, where controlled local deformation is intentionally used to create mechanical interlocking as an alternative to fusion welding.

2. Materials and Methods

2.1. Materials and Forming System

The objective of this work is to apply a slight hydroforming process to a double-layer tube composed of ST52 steel as the outer layer and GGG70 ductile cast iron as the inner layer. Following preliminary evaluations, ST52 and GGG70 were selected due to their complementary mechanical properties, while VCN150 steel was used for manufacturing the cylinder and piston components of the forming system. The chemical composition and mechanical properties of ST52 steel and GGG70 ductile cast iron are presented in Tables 1 and 2. Owing to the spherical morphology of graphite nodules, ductile cast iron exhibits improved strength, ductility, toughness, and wear resistance compared with gray cast iron [12,13].

Figure 1 illustrates the laboratory setup used for the slight hydroforming of double-walled tubes. A hydraulic jack, commonly referred to as a concrete breaker, was employed as the primary forming system. The setup consists of a hydraulic electro-pump, two opposing jaws, a restraint system, a feeding unit, a work table, and a control module. The applied forming load was generated by an AC motor, with its rotational speed regulated through a PLC-based control unit. The load values displayed by the machine (ton-force) were subsequently converted to the corresponding equivalent internal pressure (MPa) using a piston diameter of 60 mm for physical interpretation and discussion.

In this study, slight hydroforming refers to a localized, low-pressure variant of conventional hydroforming in which deformation is intentionally restricted to the interfacial region of the tube. Unlike full-forming hydroforming processes that aim to shape the entire component, slight hydroforming applies a controlled radial plastic deformation at the ST52/GGG70 interface while preserving the global geometry of the tube. This localized deformation promotes the formation of a wavy, mechanically interlocked interface, which is beneficial for interfacial stability. Accordingly, the applied forming load levels were deliberately limited to promote interfacial plasticity without inducing macroscopic geometric changes.

The purpose of the experimental program was to optimize the slight hydroforming parameters to achieve the maximum reduction in diameter (D1). For this purpose, a response surface methodology (RSM) based on a Box–Behnken design [14] was employed to evaluate the influence of three primary factors: (i) applied forming load, (ii) forming temperature, and (iii) Nano-Al_2O_3 concentration in the working fluid. To enhance lubrication during forming, Nano-Al_2O_3 particles were added to the hydraulic

fluid. The incorporation of an Al_2O_3-based nanofluid improves lubricating and load-carrying capacity through the formation of tribo-films and a micro-bearing effect induced by the nanoparticles. These mechanisms are known to reduce friction and wear, stabilize plastic flow, and improve surface quality in metal forming operations. In the context of slight hydroforming, reduced friction directly influences the transmission of radial pressure and interfacial shear stress at the ST52/GGG70 interface. Consequently, the nanofluid indirectly affects both the magnitude of diameter reduction (D1) and the resulting interfacial morphology by promoting more uniform radial deformation and a more stable interface.

For microstructural characterization, the influence of the initial interface morphology on the deformation behavior was examined using optical microscopy (OM). After sectioning, the samples were prepared following standard metallographic procedures. The cross-sections were mounted, sequentially ground using SiC papers from grit 120 to 5000, and finally polished using 1 μm and 0.25 μm diamond pastes. Optical microscopy was then performed to examine interfacial features including waviness, intermetallic layer morphology, and local deformation characteristics.

3. Experimental test Using Box-Behnken design Model

Conventional trial-and-error approaches have long been used to evaluate forming behavior and process performance; however, such methods are time-consuming and costly. Statistical design of experiments (DoE) techniques provide an efficient alternative by enabling the identification of optimal process conditions using a limited number of experiments. Among these techniques, the Box–Behnken design (BBD) is widely employed due to its capability to develop second-order response surface models without requiring extreme combinations of process parameters. The total number of experiments required in a Box–Behnken design is given by Eq. (1):

$$N = 2K(K-1) + C_0 \tag{1}$$

where N is the total number of experiments, K represents the number of factors, and C_0 denotes the number of replications at the central point of the design [15,16]. The general form of the quadratic response surface model used in this study is expressed by Eq. (2):

$$Y = b_0 + \sum_{i=1}^{k} b_i x_i + \sum_{i=1}^{k} b_{ii} x_i^2 + \sum_{i=1}^{k} \sum_{j>1}^{k} b_{ij} x_i x_j + \in \tag{2}$$

where Y is the predicted response, b_0 is the intercept, b_i, b_{ii}, and b_{ij} are the linear, quadratic, and interaction coefficients, respectively, x_i and x_j denote the coded variables, and $\in$ represents the experimental error.

The objective of this experimental design was to model and optimize the slight hydroforming parameters in order to achieve the maximum reduction in diameter (D1). Three primary factors were selected as continuous independent variables: (i) applied forming load, (ii) forming temperature, and (iii) Nano-Al_2O_3 concentration in the working fluid. To estimate pure error and assess model adequacy, three replications were performed at the central point of the design. The coded and actual levels of the selected factors are summarized in Table 3, while the complete experimental matrix generated using the Box–Behnken design is presented in Table 4.

The statistical modeling and factor coding in Design-Expert software were based on the machine-displayed forming load levels (ton-force). For physical interpretation and consistency with hydroforming literature, the corresponding equivalent internal pressure values (MPa) are reported throughout the manuscript.

The selected range of applied forming load was determined based on preliminary forming trials. The lower load level corresponds to the onset of measurable radial plastic deformation in the double-walled tube, whereas the upper level approaches the threshold beyond which localized thinning or instability may occur. The forming temperature range of 25–75 °C was chosen to provide moderate thermal softening of both ST52 steel and GGG70 ductile cast iron while avoiding microstructural phase transformations or thermal degradation.

The Nano-Al_2O_3 concentration range of 0–10 wt.% was established based on preliminary dispersion and stability tests, which indicated that higher nanoparticle concentrations led to agglomeration and sedimentation. Within this range, the nanofluid remained sufficiently stable over the duration of the experiments and enabled the potential nonlinear effects of nanoparticle content on lubrication and deformation behavior to be effectively captured by the Box–Behnken design.

4. Results and discussion

4.1. Diameter Reduction Response under Slight Hydroforming

In this study, double-walled tubular specimens composed of an outer ST52 steel layer and an inner GGG70 ductile cast iron layer was assembled and subjected to a slight hydroforming deformation process. The primary objective of this stage was to evaluate the feasibility of achieving a controlled and uniform radial contraction along the tube length through localized deformation, which is a critical requirement for deformation-assisted joining of double-layer tubular components.

During the slight hydroforming process, the applied forming load is transmitted hydrostatically through the working fluid, generating a nearly uniform radial contact pressure at the tube interface. The piston load is transferred to the outer ST52 layer

and subsequently distributed across the ST52/GGG70 interface, resulting in controlled radial plastic deformation. The greatest reduction in diameter (D1) was selected as the primary quantitative response for assessing deformation intensity and uniformity. The experimental values of D1 obtained for all Box–Behnken runs are summarized in Table 5.

4.2. RSM-Based Optimization of Diameter Reduction

A Box–Behnken response surface methodology (RSM) was employed to investigate and optimize the influence of applied forming load, forming temperature, and Nano-Al_2O_3 concentration in the hydraulic fluid on the greatest reduction in diameter (D1). A second-order polynomial model was initially developed to capture the linear, interaction, and quadratic effects of the selected parameters. The statistical adequacy of the fitted models was evaluated through sequential model testing, as summarized in Table 6.

Among the tested models, the quadratic model was identified as the most appropriate representation of the experimental data, exhibiting a high adjusted coefficient of determination and a non-significant lack-of-fit. This indicates that the selected model sufficiently captures the underlying relationship between the process parameters and the deformation response within the investigated design space.

The corrected analysis of variance (ANOVA) results are presented in Table 7. After eliminating statistically insignificant terms, all remaining model coefficients exhibited P-values below 0.05, confirming their significance. The high model F-value (78.35) further demonstrates the robustness of the developed model. Interaction between forming temperature and Nano-Al_2O_3 concentration (BC), as well as the quadratic terms of applied forming load (A^2) and temperature (B^2), were identified as significant contributors to the response.

Based on the corrected ANOVA, the reduced quadratic regression model expressed in coded variables is given by Eq. (3):

$$D_1 = +58.53 - 0.5687A - 0.1875B - 0.2513C - 0.24AB - 0.145BC + 0.3596A^2 + 0.1121B^2 \quad (3)$$

The high coefficient of determination ($R^2 = 0.9874$), in conjunction with the close agreement between the adjusted R^2 (0.9748) and predicted R^2 (0.9393), confirms the excellent predictive capability of the model. In addition, the Adeq Precision value of 26.675 significantly exceeds the recommended minimum value of 4, indicating a favorable signal-to-noise ratio and validating the suitability of the model for navigating the design space (Table 8).

4.2.1. Model Diagnostics and Response Surface Analysis

The adequacy of the developed RSM model was further assessed using diagnostic plots, including normal probability plots of residuals, residuals versus run order, residuals versus predicted values, and Box–Cox transformation plots (Figure 2). The close alignment of residuals along the reference line and the absence of systematic patterns indicate normally distributed residuals and confirm that no significant outliers or model violations are present.

The combined effects of the input parameters on the diameter reduction response are illustrated through three-dimensional response surface and two-dimensional contour plots (Figure 3). These plots provide a clear visualization of parameter interactions and nonlinear trends, enabling identification of regions associated with maximum deformation response. Standard error distributions, derived from the mean squared residual error obtained through ANOVA, were also incorporated to assess prediction uncertainty across the factor space. The consistency of contour shapes and the controlled dispersion of standard error further support the statistical reliability of the fitted model.

Perturbation plots (Figure 4) highlight the relative sensitivity of D1 to variations in each input parameter. The applied forming load exhibits the steepest slope, indicating its dominant influence on diameter reduction, followed by forming temperature and Nano-Al_2O_3 concentration. Box plots of D1 (Figure 5) further corroborate the ANOVA findings, confirming the relative contribution of each factor to the deformation response.

Figure 5 shows box plots for the greatest reduction in diameter. The box plots all confirmed the results of the all parameter effect on the response in F-value.

In the Box–Behnken design, each factor is coded at three levels (−1, 0, and +1). These coded values represent the low, medium, and high settings for each parameter involved in the experiment. In multi-response optimization, each objective can be assigned a specific weight reflecting its relative importance. Design-Expert uses an importance scale ranging from 1 (+) to 5 (+++++), with the default level set to +++. In this study, the main response of interest the greatest reduction in diameter (D1) was assigned the highest importance level (+++++) to ensure that the optimization process prioritized this parameter above others.

The desirability-based multi-response optimization method, initially proposed by Myers and Montgomery, was used to combine the individual goals into a single global desirability function. Optimization begins from randomly selected points within the design space and proceeds toward the region of steepest ascent. Because nonlinear response surfaces may contain multiple local optima, starting from multiple locations increases the likelihood of identifying the true global optimum. Graphical tools including contour plots, 3D surface plots, and perturbation plots further assist in exploring the behavior of the desirability function within the experimental domain. For each individual response, a desirability value d_i is defined, ranging from 0 (completely undesirable) to 1 (fully desirable). Each response must be assigned a target type, which can be set to None, Maximum, Minimum, Target, or Range. The overall desirability D(X) is calculated as the geometric mean of the individual desirability's, as shown in Eq. (4):

$$D = (d_1, d_2, \ldots, d_n) = \left(\prod_{i=1}^{n} d_i\right)^{\frac{1}{n}} \quad (4)$$

where n is the number of responses considered. If any individual desirability equals zero (i.e., the response falls outside its acceptable range), the overall desirability becomes zero, indicating an unacceptable solution. In this study, desirability optimization was applied to determine the optimal slight hydroforming parameters. The final desirability function used for simultaneous optimization is expressed as Eq. (5):

$$D = \left(\prod d_i\right)^{\frac{1}{n}} \quad (5)$$

Figure 6 presents the optimization results obtained from Design-Expert software for the single response D1. According to the Box–Behnken design, the optimal process parameters were identified as: pressure = 146.604 tons, temperature = 73.10 °C, and Nano-Al_2O_3 concentration = 5.5636 wt.%. Under these optimized conditions, the greatest reduction in diameter (D1) was predicted to be 57.9877 mm, representing the most favorable deformation state for the slight hydroforming of ST52/GGG70 double-walled tubes.

4.2.2. Optimization validation

To validate the statistical optimization results, confirmatory experiments were conducted at the identified optimal parameter combination. The experimental and predicted values of the greatest reduction in diameter are compared in Table 9. The deviation between the predicted and experimentally measured D1 values was below 5%, indicating good agreement and confirming the reliability of the developed RSM model and optimization strategy.

4.3. OM microscopy of the interface in the double-walled ST52/GGG70 tube

It should be noted that the OM and SEM observations presented in Figures 7 and 8 were obtained from specimens produced under the optimal parameter combination identified through the Box–Behnken optimization (Table 9). Consequently, the observed interfacial morphology characterized by a wavy interface accompanied by a thin and partly discontinuous intermetallic layer represents the microstructural manifestation of the deformation state that maximizes the greatest reduction in diameter (D1). The development of this favorable interfacial morphology is strongly governed by the applied forming parameters. Increasing the applied forming load intensifies both the normal contact pressure and interfacial shear stress at the ST52/GGG70 interface, promoting the formation of a pronounced wavy geometry and enhancing mechanical interlocking between the two layers. Forming temperature primarily influences diffusion kinetics at the interface and thus controls the thickness and continuity of the intermetallic layer. While elevated temperatures facilitate intermetallic formation, excessive growth and continuity of this brittle layer increase crack susceptibility and may compromise interfacial integrity. The optimized combination of forming load, temperature, and Nano-Al_2O_3 concentration therefore yields a balanced morphology consisting of (i) a well-developed wavy interface and (ii) a thin, segmented intermetallic layer features that are widely reported to enhance crack arrest capability and interfacial toughness in multi-material joints.

During the slight hydroforming process, local stress heterogeneities can amplify pre-existing microstructural imperfections at or near the interface. To assess the influence of intermetallic layer morphology on joint integrity, two representative interfacial conditions were examined: one exhibiting a thin and discontinuous intermetallic layer and another characterized by a thicker and more continuous layer (Figures 7a–b). In the former case, the intermetallic layer thickness ranged between approximately 5 and 10 μm (Figures 7c–d) and appeared only in isolated regions along the interface. No evidence of early-stage interfacial cracking was observed under these conditions. SEM observations of specimens subjected to slight hydroforming under optimized parameters are shown in Figure 8. Both the ST52 steel and GGG70 ductile cast iron layers experienced uniform deformation and remained mechanically bonded despite the presence of local intermetallic regions. The discontinuous nature of the intermetallic layer effectively inhibited continuous crack propagation along the interface. Instead, only short, vertically oriented microcracks were observed within the intermetallic phase, reflecting its inherently brittle behavior. These cracks did not propagate into either base material due to the ductility of ST52 steel and the geometric constraint imposed by the wavy interface.

In contrast, specimens containing a thicker and more continuous intermetallic layer exhibited a markedly different crack propagation behavior. During the final stages of deformation, microcracks formed within the continuous intermetallic film coalesced, ultimately leading to localized interfacial failure. The combined effects of brittleness and continuity promoted crack initiation and accelerated crack growth, particularly near the frontal regions of the interfacial waves where stress concentrations are highest. Nevertheless, crack propagation remained largely confined to the intermetallic layer and did not penetrate the adjacent ST52 or GGG70 layers.

A key outcome of these observations is the critical role of interface waviness in inhibiting crack propagation. Each interfacial wave acts as an individual barrier, forcing cracks to arrest or deflect rather than propagate along a continuous path. As a result, only small and isolated cracks develop within the intermetallic layer, preventing interfacial debonding. Taken together, the OM and SEM results confirm that the optimized slight hydroforming process produces a favorable interfacial morphology that enhances joint stability by combining mechanical interlocking with controlled intermetallic layer formation, rather than degrading interfacial integrity.

5. Conclusions

This study demonstrates that slight hydroforming can be effectively employed as a deformation-assisted joining technique for double-walled ST52/GGG70 tubular components when the process parameters are properly optimized. Unlike conventional tube hydroforming, the process was deliberately applied to induce controlled local plastic deformation at the interface, enabling mechanical interlocking without altering the global tube geometry. Using a Box–Behnken response surface methodology (RSM), the applied forming load, forming temperature, and Nano-Al_2O_3 concentration in the working fluid were systematically optimized to maximize the greatest reduction in diameter (D1), which serves as an indirect indicator of deformation intensity and uniformity at the interface. The optimal conditions corresponding to an applied forming load of approximately 146 ton-force (≈507 MPa equivalent internal pressure), a temperature of 73.1 °C, and a Nano-Al_2O_3 concentration of 5.56 wt.% resulted in the maximum diameter reduction while maintaining dimensional stability. The developed quadratic model exhibited excellent predictive capability, as confirmed by high R^2, adjusted R^2, and predicted R^2 values. Microstructural investigations revealed that the deformation conditions maximizing D1 directly correspond to the formation of a favorable interfacial morphology, characterized by a well-developed wavy interface and a thin, partly discontinuous intermetallic layer. This morphology plays a critical role in joint integrity: interface waviness enhances mechanical interlocking and promotes crack deflection, while the discontinuity of the intermetallic layer prevents the formation of continuous brittle paths that would otherwise accelerate crack propagation. In contrast, regions exhibiting thicker and more continuous intermetallic layers showed a higher tendency for microcrack initiation and growth during deformation. In addition, the incorporation of Nano-Al_2O_3 into the working fluid contributed to a more stable deformation regime by reducing friction and stress localization, leading to smoother response surfaces and a more regular interfacial waviness under optimized conditions. Overall, the results confirm that optimized slight hydroforming not only improves the forming response but also produces a crack-resistant and mechanically robust interface. These findings highlight the potential of slight hydroforming as a reliable alternative or complement to welding for joining dissimilar-material, double-walled tubular structures in applications where structural integrity and durability are critical.

Acknowledgments

The authors are very much thankful to the unknown reviewers for their valuable and constructive suggestions which improved the readability of the paper.

Authors' Credit

Mansourian planned the scheme, initiated the project and suggested the experiments; Mansourian and Mahmoodi conducted the experiments and analyzed the empirical results; Mansourian and Mahmoodi developed the mathematical modeling and examined the theory validation. The manuscript was written through the contribution of all authors. All authors discussed the results, reviewed and approved the final version of the manuscript.

Funding

The authors received no financial support for the research, authorship and publication of this article.

Conflicts of interest

■The authors declare that they have no known competing financial interests or personal relationships that could have appeared to influence the work reported in this paper.
□The authors declare the following financial interests/personal relationships which may be considered as potential competing interests.

References

1. Liu, M., Liu, Y., Li, H., et al. "Discontinuous yielding behavior, strengthening effect and deformation mechanism of double-wall copper-brazed steel tube under various continuous sectional cooling", *Materials Characterization*, 205, 113369 (2023). https://doi.org/10.1016/j.matchar.2023.113369.
2. Zhou, J., Qin, R., Chen, B. "Energy absorption properties of multi-cell thin-walled tubes with a double surface gradient", *Thin-Walled Structures*, 145, 106386 (2019). https://doi.org/10.1016/j.tws.2019.106386.
3. Jin, K.-Y., Deng, R., Zhou, X.-H., et al. "Compressive behavior of CFDST columns: Effects of thin-walled inner steel tubes", *Journal of Constructional Steel Research*, 214, 108443 (2024).https://doi.org/10.1016/j.jcsr.2023.108443.
4. Liu, C., Abd El-Aty, A., Lee, M.-G., et al. "Predicting the forming limits in the tube hydroforming process by coupling the cyclic plasticity model with ductile fracture criteria", *Journal of Materials Research and Technology*, 26, 109–120 (2023). https://doi.org/10.1016/j.jmrt.2023.09.022.

5. Wei, L., Xu, X., Fan, Y., et al. "Multi-step hydroforming process and wall thickness optimization of 5A02 aluminum alloy five-way tube with different branch diameters", *The International Journal of Advanced Manufacturing Technology*, 120, 6365–6375 (2022). https://doi.org/10.1007/s00170-022-09192-2.
6. Lei, Q., Li, M., Ilinich, A., et al. "Microstructural evolution and failure mechanism of an extrusion welded aluminum alloy tube during hydroforming processing", *Materials Science and Engineering A*, 756, 246–253 (2019). https://doi.org/10.1016/j.msea.2019.03.066.
7. Wang, C., Yuan, L., Wang, X. "Experimental and numerical analysis of the collapse of dented bi-metallic pipe under external pressure", *Ocean Engineering*, 319, 120187 (2025). https://doi.org/10.1016/j.oceaneng.2024.120187
8. Cui, X.L., Yuan, S.J. "Effects of superimposed hydrostatic pressure on bulging deformation and fracture of tubes in double-sided hydroforming", *Archives of Civil and Mechanical Engineering*, 19(2), 569–583 (2019). https://doi.org/10.1016/j.acme.2018.12.012.
9. Olabi, A.G., Alaswad, A. "Experimental and finite element investigation of formability and failures in bi-layered tube hydroforming", *Advances in Engineering Software*, 42(10), 815–820 (2011). https://doi.org/10.1016/j.advengsoft.2011.05.022.
10. Eraslan, A.N., Akis, T. "Deformation analysis of elastic–plastic two-layer tubes subjected to pressure: An analytical approach", *Turkish Journal of Engineering and Environmental Sciences*, 28, 261–268 (2004). https://hdl.handle.net/11511/79309.
11. Feng, Y., Jia, Y., Sun, X., et al. "Optimization of bi-layered Y-shaped tube hydroforming using response surface methodology", *The International Journal of Advanced Manufacturing Technology*, 133, 521–541 (2024). https://doi.org/10.1007/s00170-024-13726-1.
12. Megahed, H., El-Kashif, E., Shash, A.Y., et al. "Effect of holding time, thickness and heat treatment on microstructure and mechanical properties of compacted graphite cast iron", *Journal of Materials Research and Technology*, 8(1), 1188–1196 (2019). https://doi.org/10.1016/j.jmrt.2018.07.021.
13. Essam, M.A., Shash, A.Y., Megahed, H., et al. "Effect of section thickness on microstructure and mechanical properties of compacted graphite iron for diesel engine applications", *Heliyon*, 7(1), e05930 (2021). https://doi.org/10.1016/j.heliyon.2021.e05930.
14. Moghadam, H., Samimi, M., "Effect of condenser geometrical feature on evacuated tube collector basin solar still performance: Productivity optimization using a Box-Behnken design model", *Desalination*, 542, 116092 (2022). https://doi.org/10.1016/j.desal.2022.116092.
15. Yan, B., Meng, B., Ma, Y., et al. "Structural precision control with manufacturability–performance balancing for metallic thin-walled rings", *Advanced Engineering Informatics*, 65, 103307 (2025). https://doi.org/10.1016/j.aei.2025.103307.
16. Ozturk, B., "Investigation of effects of inverter frequency changes on the specific energy consumption of pipe threading susing response surface methodology", *Measurement*, 152, 107296, (2020), https://doi.org/10.1016/j.measurement.2019.107296.
17. Ghoreishi, S.R., Mahmoodi, M. "An optimized irradiation strategy and layout configuration in laser forming of copper/aluminum bi-metal sheets with functional thickness", *Proceedings of the Institution of Mechanical Engineers, Part L*, 237(6), 1394–1405 (2022). https://doi.org/10.1177/14644207221143444.
18. Kola, P.V.K.V., Pisipaty, S.K., Mendu, S.S., et al. "Optimization of performance parameters of a double-pipe heat exchanger with cut twisted tapes using CFD and RSM", *Chemical Engineering and Processing – Process Intensification*, 163, 108362 (2021). https://doi.org/10.1016/j.cep.2021.108362.
19. Norouzi, H., Mahmoodi, M. "Experimental and optimization study of compression behavior of sandwich panels with new symmetric lattice cores", *Proceedings of the Institution of Mechanical Engineers, Part L*, 236(3), 548–566 (2021). https://doi.org/10.1177/0954406220975427.
20. Chanaipoor, A., Azizi, Z., Raei, B., Tahmasebi, N., "Optimization of the thermal performance of nano-encapsulated phase change material slurry in double pipe heat exchanger: Design of experiments using response surface methodology (RSM)", Journal *of Building Engineering*, 34, 101929, (2021). https://doi.org/10.1016/j.jobe.2020.101929

Table 1: Chemical composition of ST52 steel and GGG70 cast iron materials used

Elements	Fe	C	Si	Mn	Ph	Su	Mo	Cu	Ni	Mg	Cr
ST52	Bal	0.23	0.6	1.6	0.045	0.045	--	--	--	--	--
GGG70	Bal	3.45	2.88	0.31	0.07	0.03	0.55	0.9	1.0	0.07	0.10

Table 2: Mechanical properties of ST52 steel and GGG70 cast iron materials used

Mechanical properties	Unit	Outer wall (ST52 steel)	Internal wall (GGG70 cast iron)
Density	g/cm^3	7.8	7.2
Young's modulus	GPa	210	167
Poisson's ratio	--	0.3	0.27
Yield stress	MPa	235	250
Tensile strength	MPa	370	400
Plastic strain at the point of failure	--	0.25	0.25

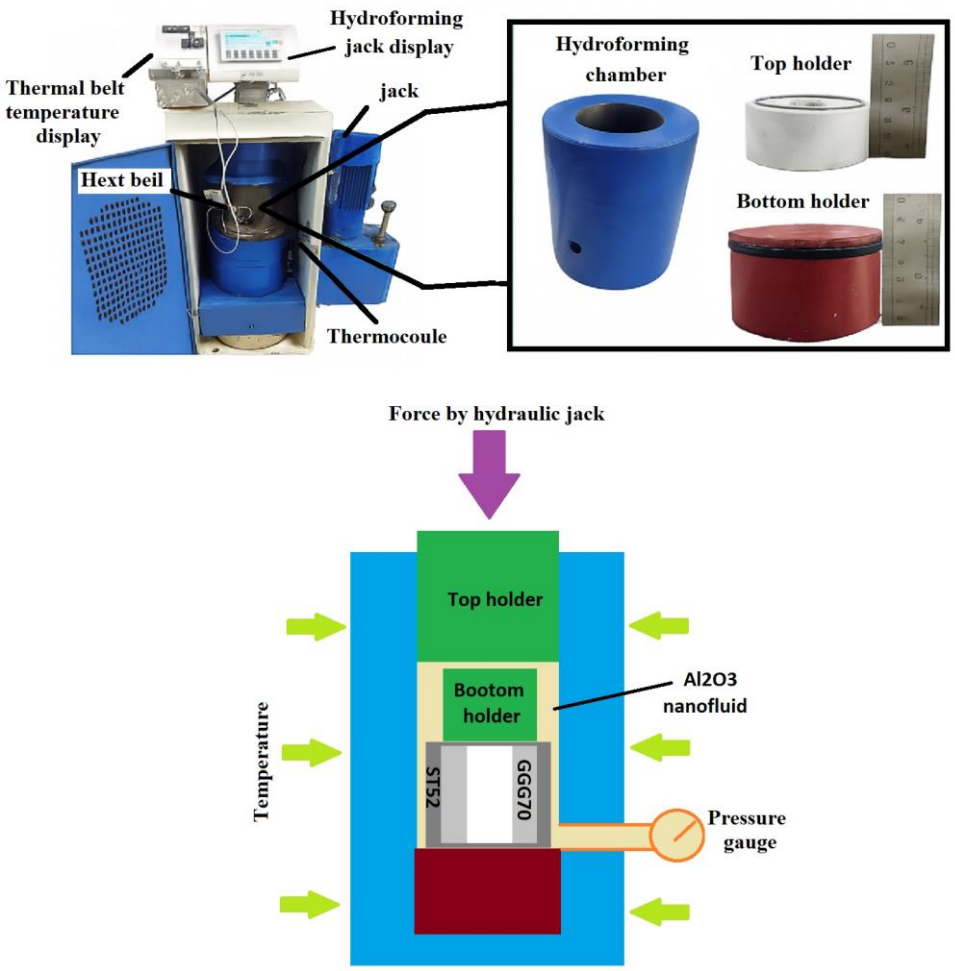

Figure 1: Laboratory equipment used in double-walled tubes of ST52 steel and GGG70 cast iron under external pressure by slight hydroforming deformation process along with process schematic

Table 3. Upper and lower levels of factors in terms of coded and uncoded symbols

NO	Welding Parameters	Units	Symbols	Range		
				Low	Medium	High
1	Force	Ton	A	50	100	150
2	Temperature	°C	B	25	50	75
3	Nano-Al2O3 percentage in fluid	%	C	0	5	10

Table 4. DoE using Box-Behnken design model

Std	Run	Input parameters		
		Force	Temperature	Nano-Al2O3 percentage in fluid
15	1	100	50	5
6	2	150	50	0
4	3	150	75	5
11	4	100	25	10
3	5	50	75	5
9	6	100	25	0
7	7	50	50	10
8	8	150	50	10
1	9	50	25	5
2	10	150	25	5
13	11	100	50	5
10	12	100	75	0
12	13	100	75	10
14	14	100	50	5
5	15	50	50	0

Table 5: Results obtained from experimental tests

Std	Run	Response
		Greatest reduction in diameter (D1) mm
15	1	58.52
6	2	58.44
4	3	58.08
11	4	58.73
3	5	59.6
9	6	58.92
7	7	59.15
8	8	58.08
1	9	59.48
2	10	58.92
13	11	58.58
10	12	58.82
12	13	58.05
14	14	58.56
5	15	59.84

Table 6: Model summary statistics of responses

Source	Sequential p-value	Lack of Fit p-value	Adjusted R^2	Predicted R^2	
Linear	0.0004	0.0096	0.7376	0.5964	
2FI	0.2428	0.0104	0.7799	0.4898	
Quadratic	**0.0007**	**0.1227**	**0.9853**	**0.9219**	**Suggested**
Cubic	0.1227		0.9969		Aliased

Table 7: ANOVA for Reduced Quadratic model

Source	Sum of Squares	df	Mean Square	F-value	p-value	
Model	**4.20**	**7**	**0.5995**	**78.35**	**< 0.0001**	**significant**
A-Pressure	2.59	1	2.59	338.17	< 0.0001	
B-Temperature	0.2812	1	0.2812	36.75	0.0005	
C-Nano-Al2O3 percentage in fluid	0.5050	1	0.5050	65.99	< 0.0001	
AB	0.2304	1	0.2304	30.11	0.0009	
BC	0.0841	1	0.0841	10.99	0.0129	
A^2	0.4803	1	0.4803	62.77	< 0.0001	
B^2	0.0467	1	0.0467	6.10	0.0428	
Residual	0.0536	7	0.0077			
Lack of Fit	0.0517	5	0.0103	11.08	0.0849	not significant
Pure Error	0.0019	2	0.0009			
Cor Total	4.25	14				

Table 8: Fit statistics and Adeq precision measures of response

Std. Dev.	0.0875	R^2	0.9874
Mean	58.78	Adjusted R^2	0.9748
C.V. %	0.1488	Predicted R^2	0.9393
		Adeq Precision	26.6750

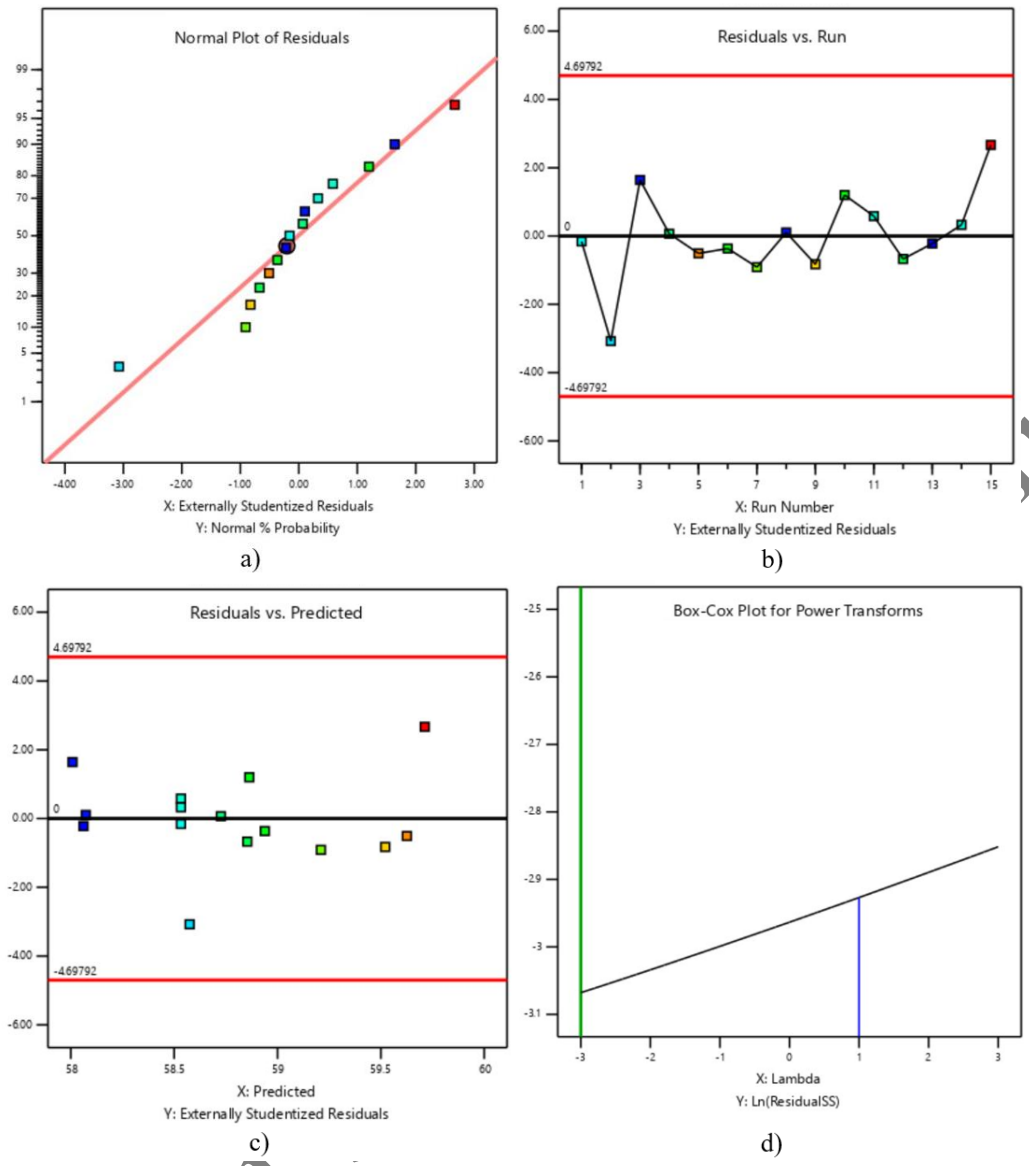

Figure 2: Diagnostics analysis of model accuracy of greatest reduction in diameter (D1): (a) Normal plot of Residuals, (b) Residuals vs. Run, (c) Residuals vs. Predicted, and (d) Box-Cox plot for power transforms

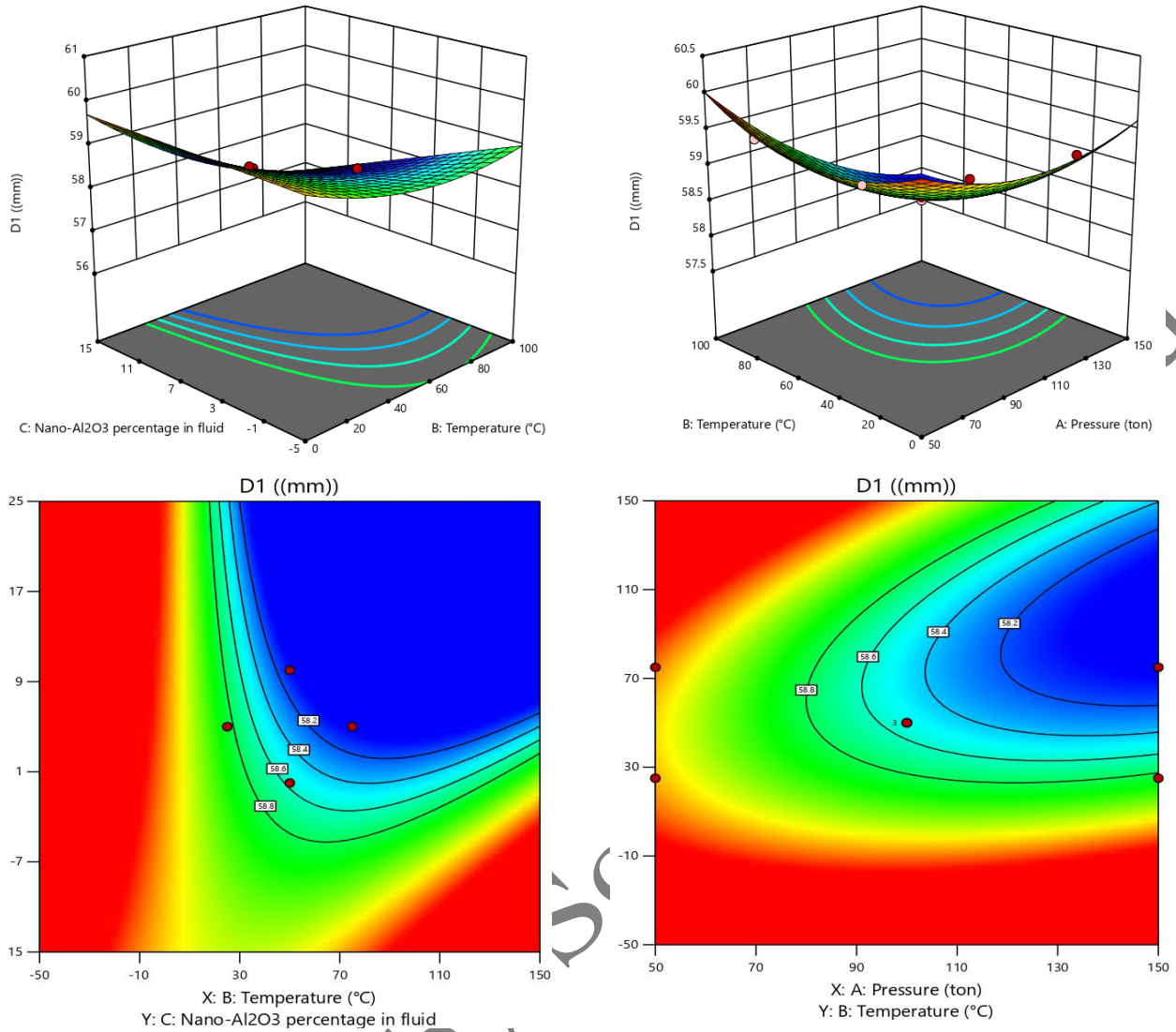

Figure 3: 3D surface and 2D contour for greatest reduction in diameter

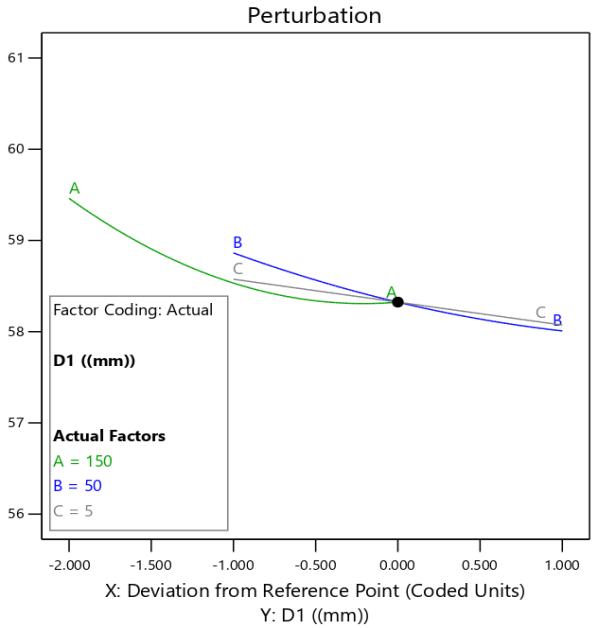

Figure 4: Perturbation Plots: greatest reduction in diameter

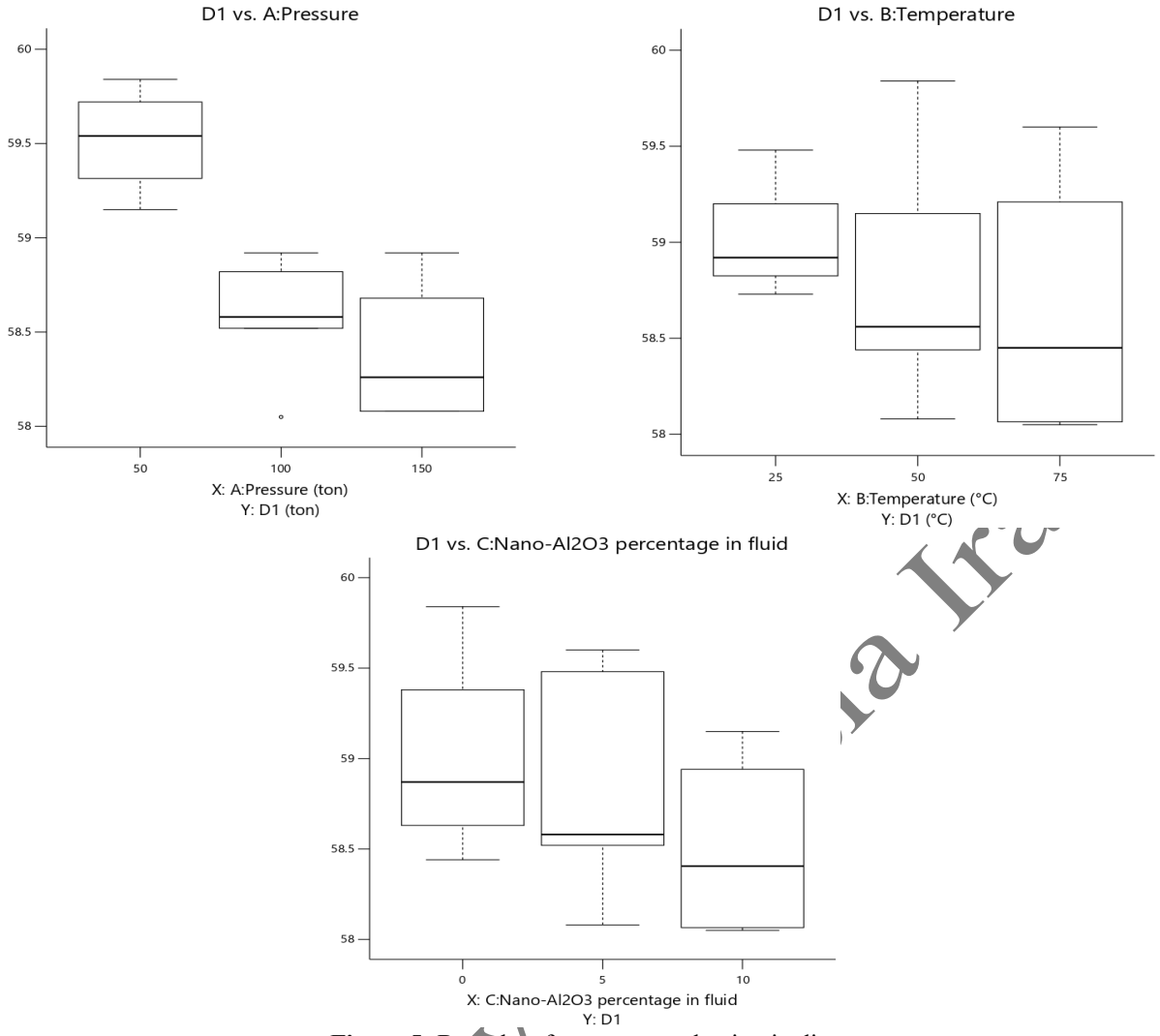

Figure 5: Box plots for greatest reduction in diameter

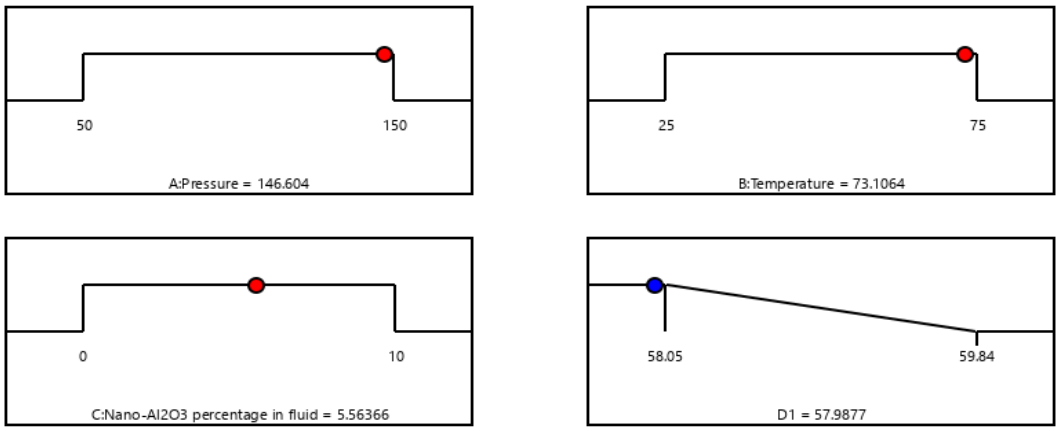

Figure 6: Results of optimization

Table 9: Validation of optimal results

Row	Pressure	Temperature	Nano-Al2O3 percentage in fluid	Greatest reduction in diameter (D1)
Optimal results	146.604	73.10	5.5636	57.9877
Validation results	146	73	5.6	58.02

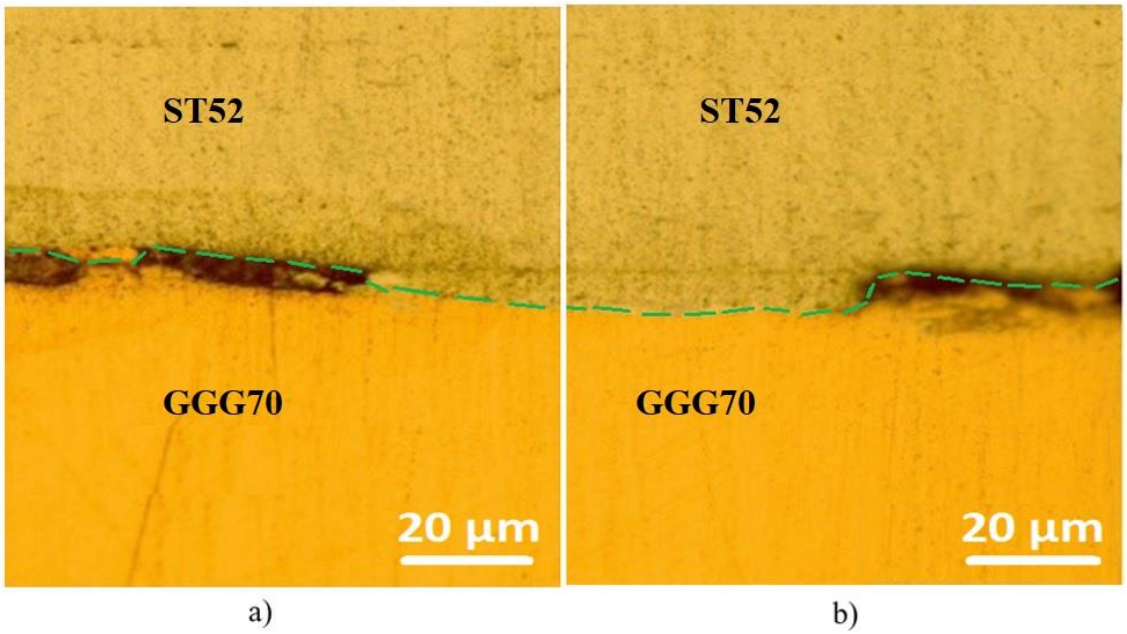

Figure 7: OM image of Interface double-walled ST52/GGG70 tube of slight hydroforming deformation process

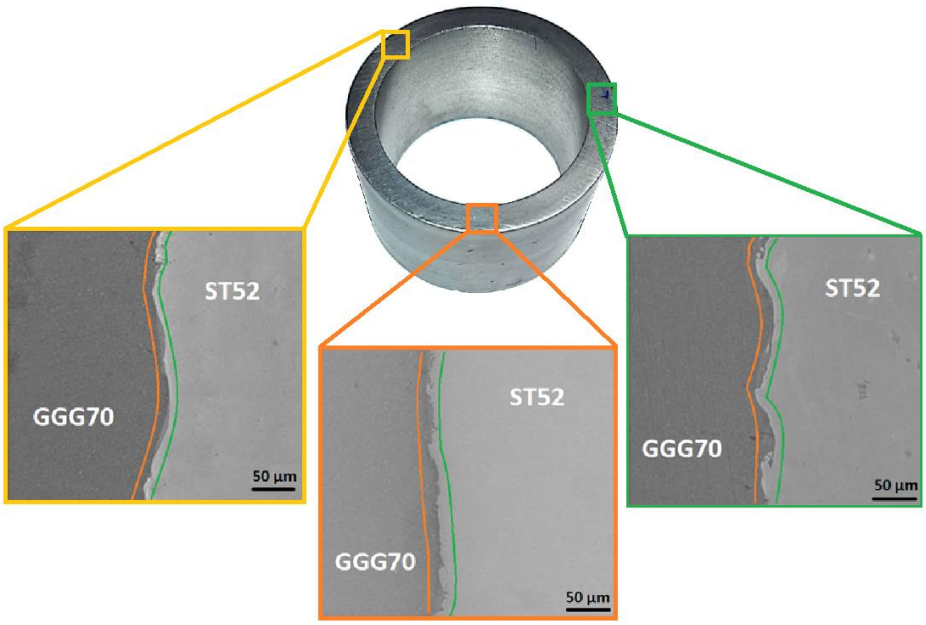

Figure 8: SEM image of Interface double-walled ST52/GGG70 tube of slight hydroforming deformation process

Biographies

Reza Mansourian is a Ph.D. student in Mechanical Engineering with a specialization in Manufacturing and Production at Semnan University, Iran. His research interests include metal forming processes, tube hydroforming, deformation-assisted joining, and optimization methods in advanced manufacturing. He holds a bachelor's and master's degree in mechanical engineering, and in addition to his engineering education, he also holds a master's degree in executive management.

Masoud Mahmoodi is an Associate Professor in the Faculty of Mechanical Engineering at Semnan University, Iran. His research focuses on material forming processes, laser forming, optimization techniques, and experimental–numerical analysis in manufacturing engineering.